RADIATION RESEARCH **202**, 862–869 (2024)
0033-7587/24 $15.00

DOI: 10.1667/RADE-23-00127.1

# Hepatic Stellate Cell-mediated Increase in CCL5 Chemokine Expression after X-ray Irradiation Determined In Vitro and In Vivo

Masataka Taga,[a,1] Kengo Yoshida,[a] Shiho Yano,[a] Keiko Takahashi,[a] Seishi Kyoizumi,[a] Megumi Sasatani,[b] Keiji Suzuki,[c] Tomohiro Ogawa,[d] Yoichiro Kusunoki,[a] Tatsuaki Tsuruyama[a,e]

[a] Department of Molecular Biosciences, Radiation Effects Research Foundation, 5-2 Hijiyama Park, Minami-ku, Hiroshima City, Hiroshima, Japan; [b] Department of Experimental Oncology, Research Institute for Radiation Biology and Medicine, Hiroshima University, Hiroshima, Japan; [c] Radiation Risk Control Unit, Atomic Bomb Disease Institute, Nagasaki University, Nagasaki, Japan; [d] Center for the Advancement of Higher Education, Faculty of Engineering, Kindai University, Hiroshima, Japan; [e] Department of Drug Discovery Medicine, Graduate School of Medicine, Kyoto University, Kyoto, Japan

**Taga M, Yoshida K, Yano S, Takahashi K, Kyoizumi S, Sasatani M, Suzuki K, Ogawa T, Kusunoki Y, Tsuruyama T. Hepatic Stellate Cell-mediated Increase in CCL5 Chemokine Expression after X-ray Irradiation Determined In Vitro and In Vivo. Radiat Res. 202, 862–869 (2024).**

**Radiation exposure causes hepatitis which induces hepatic steatosis and fibrosis. Although hepatic stellate cells (HSCs) have been considered potential pathological modulators for the development of hepatitis due to viral and microbial infections, their involvement in radiation-induced hepatitis is yet to be determined. This study aimed to clarify the relationship between radiation exposure and expressions of inflammatory cytokines and chemokines in HSCs in vitro and in vivo. HSCs were obtained from 1-week-old mice, known to be highly sensitive to radiation-induced hepatocellular carcinoma, using a newly established method combining liver perfusion, cell dissociation, and density gradient centrifugation, followed by magnetic negative selection of hematopoietic and endothelial cells with anti-CD45.2 and CD146 antibodies. The isolated HSCs were confirmed by the expression of desmin and glial fibrillary acidic protein (GFAP). We demonstrated that primary cultured HSCs, exposed to X-ray irradiation (0, 1.9, and 3.8 Gy) and cultured for 3 and 7 days, produced elevated levels of C-C motif chemokine ligand 5 (CCL5, also known as RANTES) inflammatory chemokine in a dose-dependent manner. An in vivo immunofluorescence method confirmed that increased CCL5 signals were observed in GFAP-positive HSCs in mouse livers 7 days after whole-body X-ray irradiation (1.9 and 3.8 Gy). Adequate expression of C-C motif chemokine receptor 5 (*Ccr5*), a receptor for CCL5, was also detected using real-time PCR in the liver of both irradiated and non-irradiated mice. Taken together, our data suggest that HSCs may drive hepatitis via CCL5/CCR5 axis in the liver under radiation-induced stress. Furthermore, this newly established experimental protocol can help evaluate the expression of other inflammatory cytokines in primary cultures of HSCs isolated from infant mice.** 

## INTRODUCTION

The liver can be injured owing to various factors. Hepatitis is a critical symptom of liver injury and leads to fibrosis (*1*). Hepatitis is classified as viral hepatitis, alcoholic steatohepatitis, non-alcoholic steatohepatitis, among others. Furthermore, radiation-induced liver injury (RILI) is also associated with hepatitis and is known to be an adverse effect of radiation therapy for the treatment of cancers (*2*).

Hepatic stellate cells (HSCs) are involved in inflammatory responses and liver immunology (*3*), and the modulation of HSCs is expected to be a suitable approach for treating hepatitis. HSCs are present in the Disse space between hepatocytes and sinusoidal endothelial cells and control retinol (vitamin A) storage (*4*). HSCs are activated by viral infection and liver injury and transactivate into myofibroblast-like cells with dendrites, which produce type I collagen that mediates liver fibrosis (*5*). In addition, a novel role for HSCs in regulating the inflammatory response during hepatitis has been described (*6*, *7*). Previous studies have demonstrated that HSCs promote hepatocellular carcinoma (HCC) by producing senescence-associated secretory phenotype (SASP) factors (e.g., IL-1β and IL-6) after exposure to obesity-induced gut microbial metabolites (*8*, *9*), indicating that molecular pathways linking HSCs to hepatitis may be a key to understanding the mechanisms of HCC.

Considering the involvement of HSCs in the regeneration and fibrosis of injured livers, it is reasonable to assume that HSC activation plays an important role in the development of HCC after liver injury (*10*). In an experimental radiation carcinogenesis mouse model, (C57BL/6 × C3H) F1 (B6C3F1) mice develop HCC after whole-body irradiation with high reproducibility, especially in infants (*11*, *12*), providing an ideal model for examining the mechanism by which HSCs are involved in HCC development.

To date, adult HSCs have been isolated using a combination of pronase-collagenase perfusion and density gradient centrifugation (*13*, *14*). Although one study attempted to isolate HSCs from fetal mice using an anti-p75 neurotrophin receptor

[1] Address for correspondence: Department of Molecular Biosciences, Radiation Effects Research Foundation; email: taga@rerf.or.jp.

antibody and subsequent cell sorting (*15*), HSC isolation from infants has never been reported. In this study, we developed a new isolation method including modified perfusion of the infant liver, density gradient centrifugation, and magnetic bead cell separation, to facilitate in vitro HSC analysis of the infant mouse livers. Using this method, we analyzed the expression of inflammatory cytokines and chemokines after X-irradiation in the primary HSCs isolated from 1-week-old mice, and confirmed the results in vivo.

## MATERIALS AND METHODS

### *Mice*

B6C3F1 mice were obtained from a cross between C57BL/6N (The Jackson Laboratory Japan Inc., Yokohama, Japan) and C3H/HeJ (Japan SLC Inc., Hamamatsu, Japan) mice and bred under specific pathogen-free (SPF) conditions at the animal facility at the Radiation Effects Research Foundation (RERF). All mice were fed a regular diet ad libitum. All animal experiments were approved by the Experimental Animal Care Committee of the RERF.

### *Histological Analysis of Radiation Response in Mouse Livers*

One-week-old male mice were irradiated with 0, 1.9, and 3.8 Gy X rays. One week later, the mice were euthanized by isoflurane inhalation and blood was removed from the livers and livers were collected. The livers were then embedded in optimal cutting temperature (OCT) compound, and quickly frozen in dry ice-acetone. Frozen 5-μm OCT-embedded liver sections were prepared, air-dried, and fixed with 4% paraformaldehyde (PFA) for 10 min. The fixed sections were stained with hematoxylin and eosin. A histological evaluation was performed by a pathologist.

### *Isolation of HSCs from 1-Week Old Mice*

To isolate HSCs from 1-week-old B6C3F1 mice, female and male mice from the same litter were used. The B6C3F1 mice were euthanized by isoflurane inhalation, after which a 22 G winged needle was inserted into the inferior vena cava under a stereomicroscope. The liver was then perfused with SC-1 solution (*16*) for 2 min (3.5 mL/min). In 1-week-old mice, perfusion with SC-2 solution (*16*), including pronase and collagenase destroyed the liver due to over digestion. Therefore, perfusion with SC-1 solution containing ethylene glycol tetra-acetic acid (EGTA), instead of pronase and collagenase, was performed. After SC-1 perfusion, the livers were collected in a dish with SC-2 solution containing 0.67 mg/mL pronase E (Merck Millipore, Burlington, MA), 0.67 mg/mL collagenase (Fujifilm Wako Pure Chemical Corporation, Osaka, Japan), and 17 μg/mL DNase (Fujifilm Wako Pure Chemical Corporation). The livers were then cut into approximately 1 mm squares with scissors, followed by cell dissociation in the SC-2 solution (up to 48 mL) with stirring at 37°C for 30 min. Dissociated cells were filtered through a cell strainer (70 μm nylon; Corning Inc., Corning, NY). Solutions for density gradient centrifugation were prepared according to a previously described protocol (*13*), with some modifications. Briefly, a pellet of liver-dissociated cells was suspended in 25 mL of 13% Histodenz solution. The 25 mL Histodenz solution consisted of Gey's balanced salt solution B (GBSS/B) (finally added up to 25 mL) with phenol red and a pre-filtered mixture of 3.25 g of Histodenz (Sigma-Aldrich Co. LLC, St. Louis, MO) and 7 mL of Gey's balanced salt solution A (GBSS/A) with phenol red. The Histodenz solution containing cells were divided into two tubes, layered with 1 mL of GBSS/B solution, and centrifuged at 1,300 × *g* for 15 min at 20°C. After centrifugation, cells were collected from the total Histodenz solution, except for the cell pellet. Regarding density gradient centrifugation, 8% Histodenz was not suitable for the isolation of HSCs from infant mice, resulting in no floating cells. Therefore, 13% Histodenz was adopted. The cells included in the Histodenz solution were collected under these conditions. It is possible that hematopoietic and/or sinusoidal endothelial cells were present in the floating cells. Hematopoietic cells were removed by anti-CD45.2 antibody and magnetic beads, and sinusoidal endothelial cells were removed using anti-CD146 antibody and magnetic beads, respectively. Specifically, the collected cells after the 13% Histodenz density gradient centrifugation were then incubated with purified rat anti-mouse CD16/CD32 antibody (BD Biosciences, San Jose, CA) at 4°C for 10 min to block Fc receptors, and then incubated with biotin conjugated anti-mouse CD45.2 antibody (Miltenyi Biotec, Bergisch Gladbach, Germany) and biotin conjugated anti-mouse CD146 (LSEC) antibody (Miltenyi Biotec) at 4°C for 15 min. After washing, the cells were incubated with anti-Biotin MicroBeads UltraPure (Miltenyi Biotec) at 4°C for 15 min and separated using the autoMACS Pro Separator (Miltenyi Biotec). Possel 2 program was used to run the autoMACS Pro Separator. Cells from the negative fraction were collected and used in experiments.

### *Primary Culture of Isolated HSCs*

Isolated HSCs were cultured in Dulbecco's Modified Eagle Medium (DMEM) containing 10% fetal bovine serum (FBS) at 37°C in a 5% $CO_2$ incubator (FORMA STERI-CYCLE i160, Thermo Fisher Scientific, Waltham, MA). Overnight cultured cells were pipetted into the culture medium, and floating cells were removed by medium exchange, leaving only adherent cells.

### *Immunofluorescence Analyses of HSCs*

Cells were seeded on poly L-lysine-coated cover glasses placed in 35-mm tissue culture dishes. Adherent cells were cultured, and 4% PFA fixation was performed for 20 min at room temperature. The cells were permeabilized with 0.5% Triton X-100 in PBS for 20 min at room temperature. Blocking was performed with 10% normal goat serum for 15 min at room temperature. Cells were incubated with Alexa Fluor 488 conjugated anti-glial fibrillary acidic protein (GFAP) antibody (clone: GA5, Thermo Fisher Scientific) and Alexa Fluor 647 conjugated anti-desmin antibody (clone: Y66, Abcam, Cambridge, UK) at 4°C overnight. Cells were stained with 4′,6-Diamidino-2-Phenylindole, Dihydrochloride (DAPI), mounted, and observed using the BZ-X710 All-in-one fluorescence microscope (Keyence, Osaka, Japan).

### *Flow Cytometry for HSCs*

Cultured adherent cells were harvested by trypsinization, and 4% PFA fixation was performed for 20 min at room temperature. The cells were permeabilized with 0.5% Triton X-100 in PBS for 20 min at room temperature. After incubation with Alexa Fluor 488 conjugated anti-GFAP antibody (clone: GA5, Thermo Fisher Scientific) and Alexa Fluor 647 conjugated anti-desmin antibody (clone: Y66, Abcam) at 4°C overnight, the cells were analyzed using the MACSQuant Analyzer 10 (Miltenyi Biotec). Autofluorescence of the cells was detected using a V1 filter (450/50 nm). Flow cytometric data were analyzed using FlowJo software (version 10.8.1; BD Biosciences).

### *X-ray Irradiation*

HSCs cultured overnight, pipetted, and media changed were subjected to 0, 1.9, and 3.8 Gy of X-ray irradiation (0.884 Gy/min) using the Faxitron CP-160 (Faxitron X-Ray Corp., Wheeling, IL), and the culture medium was immediately changed after X-ray irradiation.

### *Quantification of Gene Expression in HSCs*

Gene expression in HSCs was quantified using real-time RT-PCR. After X-ray irradiation analysis on days 3 and 7, $2 \times 10^5$ cells and $1 \times 10^5$ cells were initially seeded onto 35-mm tissue culture dishes, respectively. RNA was extracted from primary cultured HSCs with TRIzol Reagent (Thermo Fisher Scientific) and Direct-zol RNA MicroPrep (Zymo Research, Irvine, CA), and reverse-transcribed to cDNA with the PrimeScript RT Master Mix (Takara Bio Inc., Kusatsu, Japan). Using the cDNA samples, gene expression was quantified using the QuantStudio 7 Flex Real-Time PCR System (Thermo Fisher Scientific) with Brilliant III Ultra-Fast SYBR Green QPCR Master Mix (Agilent Technologies, Inc.,

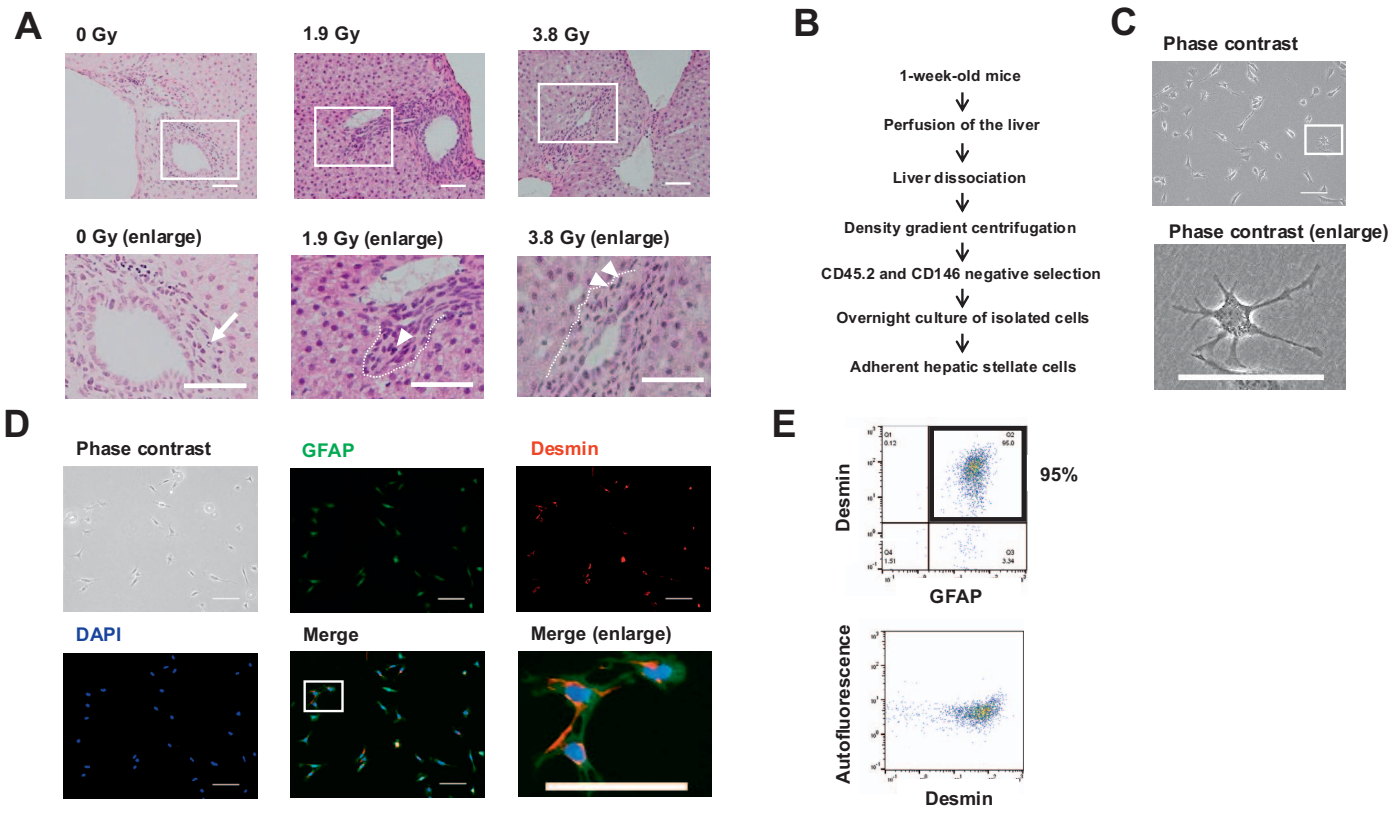


**FIG. 1.** Isolation of hepatic stellate cells (HSCs) from 1-week-old mice. Panel A: Hematoxylin and eosin-stained liver tissue sections from 1-week-old mice after 1 week of 0, 1.9, and 3.8 Gy X-ray irradiation. The area squared in white in the top panel is enlarged in the bottom panel. The main infiltrating cells in the liver tissue sections without irradiation (labeled as 0 Gy), are neutrophils, indicated by an arrow. In the histological images of the Glisson's sheaths of liver sections exposed at 1.9 Gy and 3.8 Gy irradiation (labeled as 1.9 Gy, 3.8 Gy), destruction of the limiting plate is indicated by dotted lines, and lymphocytes are indicated by arrowheads. Scale bars = 50 μm. Panel B: Outline of the experimental protocol used for HSC isolation. Panel C: Examples of the overnight primary cultures of cells isolated from the mice. The cells isolated cells from 1-week-old mice were primarily cultured overnight. The cultured cells were pipetted onto culture dishes, and the floating cells were removed by medium exchange, leaving behind only the adherent cells. The area squared in white in the top panel is enlarged in the bottom panel. Scale bars = 100 μm. Panel D: Examples of assessment of isolated cells by immunofluorescence staining. Cells isolated from 1-week-old mice were cultured overnight and assessed by immunofluorescence staining. GFAP and desmin are hepatic stellate cell markers. Scale bars = 100 μm. The area squared in white in the merged center panel is enlarged in the bottom-right panel. Panel E: Assessment of the purity of isolated cells using flow cytometry. The isolated cells were cultured overnight. The purity of the primary cultured cells was assessed by GFAP and desmin markers using flow cytometry. Autofluorescence, another HSC marker, was also analyzed. GFAP, glial fibrillary acidic protein; DAPI, 4′,6-diamidino-2-phenylindole, dihydrochloride.

Santa Clara, CA) and appropriate gene primer sets. Primer sequences for the glyceraldehyde-3-phosphate dehydrogenase (*Gapdh*) gene were as follows: forward, 5′-CAACTACATGGTCTACATGTTC-3′ and reverse, 5′-CACCAGTAGACTCCACGAC-3′. For the C-C motif chemokine ligand 5 (*Ccl5*) gene, the primers used were as follows: forward, 5′-GCTGCTTTGCCTACCTCTCC-3′ and reverse, 5′-TCGAGTGACAA ACACGACTGC-3′. For the growth differentiation factor 15 (*Gdf15*) gene, the primers were forward: 5′-CCGAGAGGACTCGAACTCAG-3′ and reverse: 5′-GGTTGACGCGGAGTAGCAG-3′. For the C-X-C motif chemokine ligand 1 (*Cxcl1*) gene, the primers were forward: 5′-GCTGGGATTCACCTCAAGAA-3′ and reverse: 5′-AGGTGCC ATCAGAGCAGTCT-3′. For the *p21* gene, the primers were forward: 5′-TCGCTGTCTTGCACTCTGGTGT-3′ and reverse: 5′-CCAAT CTGCGCTTGGAGTGATAG-3′. The expression levels of *Ccl5*, *Gdf15*, *Cxcl1*, and *p21* relative to *Gapdh*, were calculated using delta Ct values (*17*).

### *Quantification of Secreted Cytokines*

The secreted cytokines were quantified using a cytokine array. One hundred thousand HSCs were seeded into 35 mm tissue culture dishes and cultured for 7 days after X-ray irradiation without further medium change. When the culture dish supernatant was collected, the number of cells was counted to compensate for the total supernatant produced during quantification of the secreted cytokines. In this case, a compensatory amount of the supernatant from 20,000 cells was used. Secreted cytokines (e.g., IL-1β, IL-6, TNF-α, and CCL5) from primary cultured HSCs were quantified using the Proteome Profiler Mouse XL Cytokine Array Kit (R&D Systems, Minneapolis, MN), according to the manufacturer's instructions. The chemiluminescent signals from each spot on the membranes were visualized using an ImageQuant LAS 4000 mini-imaging system (GE Healthcare, Chicago, IL).

### *Quantification of Secreted CCL5*

Quantification of secreted CCL5 from primary cultured HSCs was performed using the Quantikine ELISA Mouse/Rat CCL5/RANTES Immunoassay Kit (R&D Systems), following the manufacturer's instructions. After X-ray irradiation analyses on days 3 and 7, $2 \times 10^5$ and $1 \times 10^5$ cells were initially seeded into 35-mm tissue culture dishes, respectively. The cell culture was continued for 3 or 7 days after X-ray irradiation without further medium change. When the culture dish supernatant was collected, the cells were counted to compensate for the quantification of secreted cytokines. POWERSCAN HT (BioTek Instruments, Winooski, VT) and Multiskan FC (Thermo Fisher Scientific) microplate readers were used to measure absorbance at 450 nm.

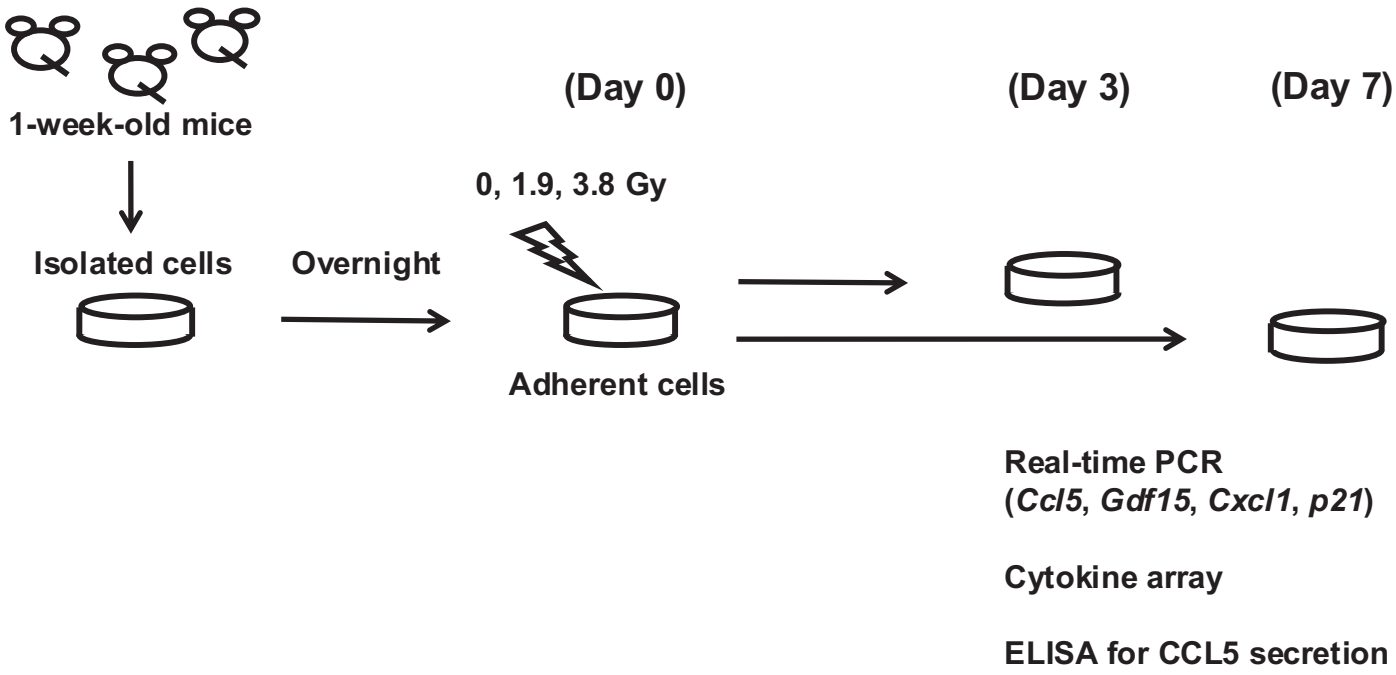


**FIG. 2.** Outline of the experimental protocol for inflammatory cytokine expression analyses. Cytokine array experiments were performed 7 days after in vitro X-ray irradiation (0 and 3.8 Gy). *Ccl5*, C-C motif chemokine ligand 5; *Gdf15*, growth differentiation factor 15; *Cxcl1*, C-X-C motif chemokine ligand 1.

*Immunofluorescence Analysis of CCL5 Expression in Mouse Livers*

The frozen OCT-embedded livers were prepared from male mice 1 week after irradiation with 0, 1.9, and 3.8 Gy X rays. Then, 5-μm sections from the frozen OCT-embedded livers were prepared, air-dried, and fixed with acetone on ice for 10 min. The sections were then blocked by 10% normal goat serum for 15 min at room temperature and incubated with Alexa Fluor 488 conjugated anti-GFAP antibody (clone: GA5, Thermo Fisher Scientific) and anti-CCL5 antibody (clone: 25H14L17, Thermo Fisher Scientific) at 4°C overnight. Then, Alexa Fluor 647 conjugated anti-rabbit IgG antibody (Cell Signaling Technology, Danvers, MA) was added at 37°C for 3 h. Sections were stained with DAPI, mounted, and observed using the BZ-X710 All-in-one fluorescence microscope (Keyence).

*Statistical Analyses*

Statistical analyses were performed using IBM SPSS Statistics (version 28; IBM, Chicago, IL). All values in bar graphs are represented as mean ± SD. P-trend values were obtained using the Jonckheere-Terpstra trend test.

## RESULTS

*Isolation of HSCs from 1-Week-Old Infant Mice*

The radiation response of the livers of 1-week-old mice was examined histologically (Fig. 1A). In the livers of non-irradiated mice (0 Gy), non-specific neutrophil infiltration was observed in the Glisson's sheaths (Fig. 1A). Furthermore, non-specific lymphocyte infiltration was observed in the liver tissues without the destruction of the limiting plate. However, in the livers of mice exposed to 1.9 Gy of X rays, a significant increase in interface hepatitis was observed, characterized by severe lymphocytic infiltration within the Glisson's sheaths and accompanied by the destruction of the limiting plate (Fig. 1A and Supplementary Fig. S1;[2] https://doi.org/10.1667/RADE-23-00127.1.S1). In the livers of mice exposed to 3.8 Gy of X rays, the degree of interface hepatitis was lower compared to that observed at 1.9 Gy; yet, the destruction of the limiting plate persisted (Fig. 1A and Supplementary Fig. S1). We developed a novel method (Fig. 1B) to isolate HSCs from one-week-old mice. The mean number of mice used for the HSC isolations was 6.6 (SD = 2.2). The number of cells isolated after negative selection is shown in Supplementary Fig. S2 (https://doi.org/10.1667/RADE-23-00127.1.S1). The calculated mean number of isolated cells from one mouse was more than 100,000 and tended to increase with the weight of the mouse. Some isolated cells showed a star-like shape, similar to that of adult HSCs (Fig. 1C). Characterization of the isolated cells was performed by immunofluorescent staining of the HSC markers, GFAP, and desmin (*18*, *19*). Isolated HSCs were cultured overnight, and the expression of GFAP and desmin was observed (Fig. 1D). The purity of these adherent primary cultured cells was assessed using flow cytometry for GFAP, desmin, and autofluorescence. These results indicated that the purity of the HSCs was > 90% (Fig. 1E).

*Analysis of Inflammatory Cytokine Expression in Cultured HSCs after In Vitro Irradiation*

Cytokine expression was examined in the isolated HSCs cultured for 3 and 7 days after X-ray irradiation (Fig. 2).

[2] Editor's note. The online version of this article (DOI: https://doi.org/10.1667/RADE-23-00127.1) contains supplementary information that is available to all authorized users.

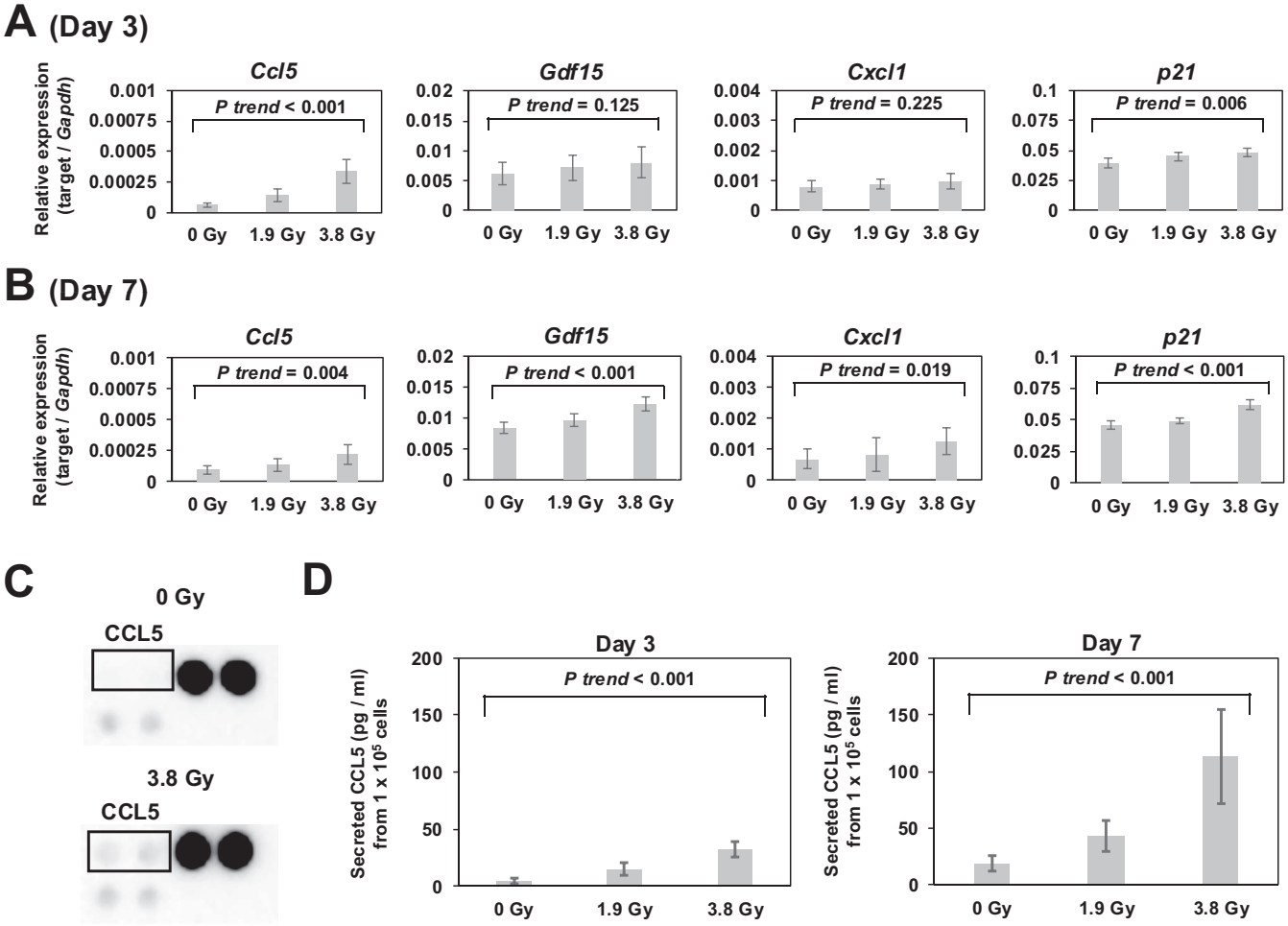


**FIG. 3.** Analysis of inflammatory cytokine expression in cultured hepatic stellate cells (HSCs) after in vitro irradiation. Panel A: Real-time PCR assessment of gene expression levels in cultured HSCs 3 days after in vitro X-ray irradiation. Panel B: Real-time PCR assessment of gene expression levels in cultured HSCs 7 days after in vitro X-ray irradiation. The vertical axis demonstrates the relative expression of each target gene per *Gapdh* gene. All values are represented as mean ± SD. All P-trend values were calculated using the Jonckheere-Terpstra trend test. These data were obtained from six experiments. Panel C: A representative image of cytokine array for secreted CCL5 protein levels in cultured HSCs 7 days after in vitro X-ray irradiation. The top and bottom images indicate 0 and 3.8 Gy samples, respectively. The left bottom two black spots below CCL5 are spots for CD40. The right two black spots are control spots. This cytokine array experiment was repeated in triplicate. Panel D: ELISA quantification of secreted CCL5 protein levels in cultured HSCs 3 and 7 days after in vitro X-ray irradiation. The left and right figures indicate samples from days 3 and 7 after X-ray irradiation, respectively. All values are represented as mean ± SD. All P-trend values were calculated using the Jonckheere-Terpstra trend test. These data were obtained from six experiments. *Gapdh*, glyceraldehyde-3-phosphate dehydrogenase; *Ccl5*, C-C motif chemokine ligand 5; *Gdf15*, growth differentiation factor 15; *Cxcl1*, C-X-C motif chemokine ligand 1.

Real-time PCR assessment of the cytokine genes, *Ccl5* (*20*), *Gdf15* (*21*), and *Cxcl1* (*Gro-α*) (*9*), and senescence-associated gene, *p21* (*9*). Significant increases in *Ccl5* and *p21* expression levels with radiation dose was observed at 3 (Fig. 3A) and 7 days (Fig. 3B) after X-ray irradiation. Of the genes examined, the expression of *Ccl5* in HSC increased more than threefold on day 3 after irradiation with 3.8 Gy X rays, which was the most significant increase. We then investigated cytokine expression profiles using cytokine arrays, which demonstrated increased secretion of CCL5 (Fig. 3C) after exposure to 3.8 Gy X rays. In contrast, radiation-associated increases in IL-1β, IL-6, and TNF-α secretion were not observed (Supplementary Fig. S3; https://doi.org/10.1667/RADE-23-00127.1.S1). ELISA was performed to quantify secreted and accumulated CCL5 protein levels in the culture medium of HSCs (Fig. 3D), and secretion of CCL5 protein was significantly upregulated at 3 and 7 days after in vitro X-ray irradiation (Fig. 3D).

### *Analyses of CCL5 Protein Expression in the Liver after In Vivo Irradiation*

CCL5 protein expression was also confirmed by immunofluorescence in the liver 1 week after in vivo irradiation in 1-week-old mice (Fig. 4). We observed an increased expression of GFAP and CCL5 after exposure to 1.9 and 3.8 Gy X rays. Furthermore, GFAP-positive cells expressed CCL5. Expression of C-C motif chemokine receptor 5 (*Ccr5*), a CCL5 receptor, was also examined by real-time PCR using RNA obtained from the livers of X-ray irradiated mice. Although *Ccr5* was expressed in the liver, no change was

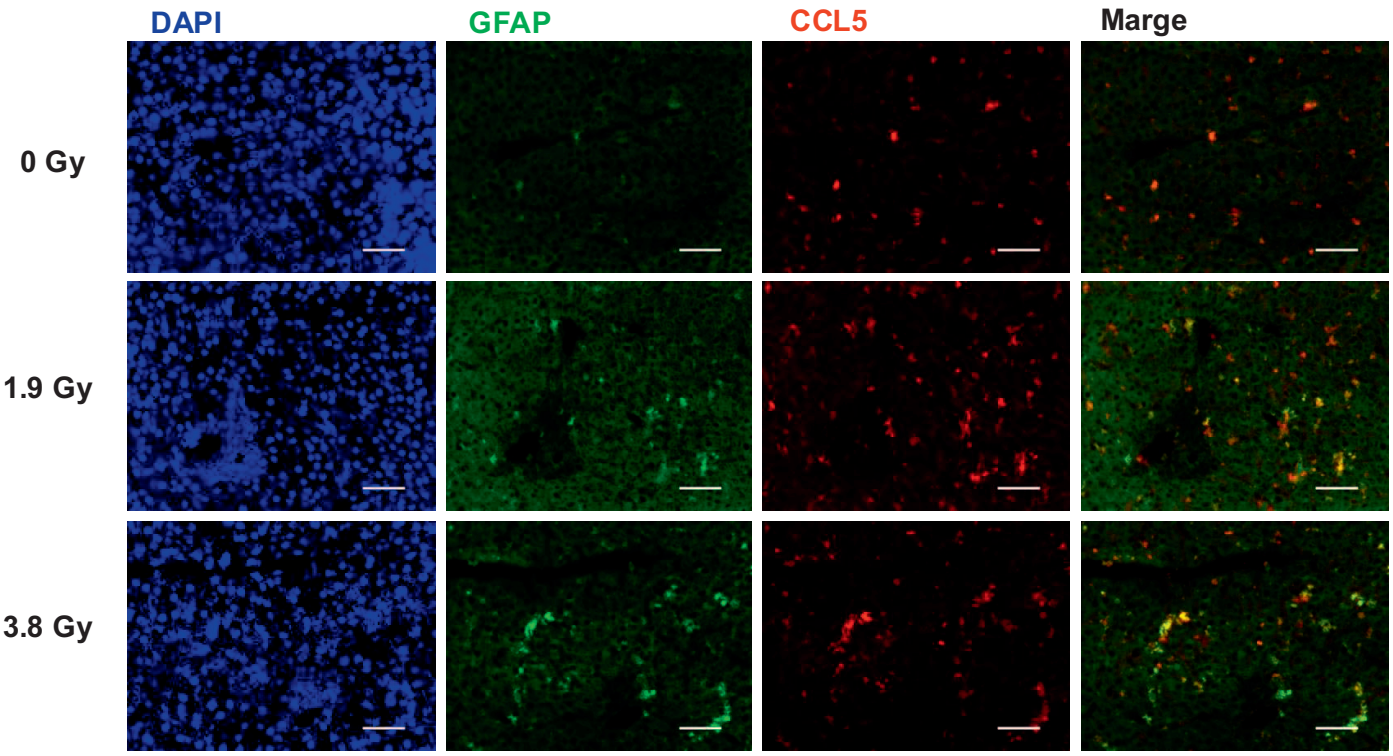


**FIG. 4.** Analyses of CCL5 protein expression in the liver after in vivo irradiation. Examples of GFAP and CCL5 protein expression in liver sections 1 week after 0, 1.9, and 3.8 Gy X-ray irradiation in 1-week-old mice. GFAP is an HSC marker. Scale bars = 50 μm. DAPI, 4′,6-diamidino-2-phenylindole, dihydrochloride; GFAP, glial fibrillary acidic protein; CCL5, C-C motif chemokine ligand 5.

observed in relation to radiation dose (Supplementary Fig. S4; https://doi.org/10.1667/RADE-23-00127.1.S1 and Supplementary Materials and Methods; https://doi.org/10.1667/RADE-23-00127.1.S2).

## DISCUSSION

To date, no studies have focused on isolated HSCs in mouse models of RILI (*2*). One reason for this could be the difficulty of isolating HSCs from infant mouse livers. In the present study, we established a new isolation method for HSCs from 1-week-old mice, which enabled the direct observation of enhanced CCL5 expression in HSCs in response to X-ray irradiation in vitro. Increased fluorescence intensity of CCL5 was also observed in infant mouse liver tissue sections, confirming the usefulness of this new isolation method for investigating the molecular responses of HSCs both in vitro and in vivo. Similar to a recent report by Chen (*22*), we observed the induction of CCL5 expression in HSCs by irradiation in our experimental system. Notably, an increased GFAP fluorescence intensity was observed in the same liver tissue sections. Whether this observation was due to increased expression of GFAP in the HSCs or to the accumulation of GFAP-expressing HSCs should be clarified by using isolated HSCs in the future.

HSCs isolated from 1-week-old B6C3F1 mice were irradiated with X rays at doses of 0, 1.9, and 3.8 Gy. Because 1.9 and 3.8 Gy X-ray irradiation is known to increase the incidence of HCC in B6C3F1 mice (*11*, *12*, *23*), and the increased excess relative risk of HCC with radiation dose among atomic-bomb survivors was observed at similar dose levels (*24*), the results obtained from our study may be applicable to human cases, proposing that 1.9 Gy X-ray irradiation of human HSCs could increase the expression of CCL5. After X ray (0, 1.9, and 3.8 Gy) exposure in vitro, primary cultured HSCs produced elevated levels of the inflammatory chemokine CCL5, in a dose-dependent manner. However, severe lymphocytic infiltration was observed after 1.9 Gy X-ray exposure, as opposed to exposure to 3.8 Gy X rays in vivo. Although we do not have data to explain the reasons for this observation, we hypothesize that 3.8 Gy X rays may directly damage lymphocytes, resulting in lower lymphocytic infiltration. In addition, the livers of 3.8 Gy X-irradiated mice were smaller than those of 0 and 1.9 Gy irradiated mice (data not shown), suggesting that hepatocytes may also be severely affected by 3.8 Gy X-irradiation. In other words, liver damage and the associated inflammatory response caused by 3.8 Gy X-irradiation may be different to that caused by the 1.9 Gy X-irradiation. Primary cultured HSCs were 7.6 Gy irradiated during a preliminary experiment. Owing to a decrease in cell proliferation ability of hepatic stellate cells and an increase in cell death after 7.6 Gy irradiation (data not shown), the 7.6 Gy irradiation experiment was not suitable.

CCL5 is a CC-chemokine secreted by hepatocyte populations, including hepatocytes, macrophages, sinusoidal endothelial cells, and HSCs (*20*, *25*, *26*). The interaction between CCL5 and CCR5 is known as the CCL5/CCR5 axis, which

is involved in the PI3K/AKT/mTOR pathway and is an essential inflammatory pathway in the liver (*27*). CCL5 may recruit T cells and/or monocytes via CCR5 during the early phase of hepatitis. Consequently, CCL5 exacerbates the inflammatory response, which explains why its increase is involved in various pathologies, including acute hepatitis, hepatic reperfusion injury, chronic viral hepatitis, alcoholic liver disease, nonalcoholic fatty liver disease, and fibrosis. Radiation is known to increase the expression of CCL5 in different cells (e.g., mouse embryonic fibroblasts and macrophages) from HSCs (*28*, *29*). In particular, the cGAS-STING pathway, which regulates innate immunity induced by DNA damage, has been implicated in the production of CCL5 (*30-32*). Because irradiation induces DNA damage, this pathway may be related to HSC-induced hepatitis. However, the development and phenotype of radiation-induced HSC-mediated hepatitis are poorly understood. Therefore, our novel experimental system is expected to provide detailed information for clarifying these mechanisms.

Whether radiation-induced CCL5 expression directly affects hepatocytes remains unclear. The CCL5/CCR5 axis is associated with the migration and invasion of HCC cells (*33*). Furthermore, HSCs induce hepatocyte steatosis via CCL5 chemokine secretion (*20*). Depletion of HSCs inhibits hepatic steatosis in mice (*34*). Maraviroc, a CCR5 antagonist, (anti-HIV drug) suppresses HCC development (*35*). If the induction of CCL5 expression by radiation is significantly associated with fatty liver and liver fibrosis, inhibition of the CCL5/CCR5 axis by maraviroc could prevent radiation-related HCC.

Finally, it should be mentioned that our new isolation method is applicable not only to the study of the effects of radiation on HSCs but also to the analysis of the effects of other factors, such as chemicals. A similar method for the isolation of HSCs was reported (*36*) during the preparation of this data. Our methods could be further improved with information from this study.

## SUPPLEMENTARY MATERIALS

Supplementary materials and methods. Quantification of C-C motif chemokine receptor 5 (*Ccr5*) gene expression in the liver.

Supplementary Fig. S1. Quantification of interface hepatitis in liver tissue sections 1 week after X-ray irradiation in 1-week-old mice.

Supplementary Fig. S2. Number of isolated HSCs per mouse.

Supplementary Fig. S3. Representative images for secreted IL-1β, IL-6, and TNF-α protein levels in cultured hepatic stellate cells 7 days after in vitro X-ray irradiation.

Supplementary Fig. S4. Analyses of *Ccr5* gene expression in the liver after in vivo irradiation.

## ACKNOWLEDGMENTS

The Radiation Effects Research Foundation (RERF), Hiroshima and Nagasaki, Japan, is a public interest foundation funded by the Japanese Ministry of Health, Labour, and Welfare and the U.S. Department of Energy to conduct research and studies for peaceful purposes on medical effects of radiation and associated diseases in humans, to contribute to the health and welfare of atomic bomb survivors and all humankind. The views of the authors do not necessarily reflect those of the two governments. This work was partially supported by the Program of the Network-Type Joint Usage/Research Center for Radiation Disaster Medical Science. The authors thank Dr. A. Noda, Dr. K. Hamasaki, Mr. K. Koyama, and Mr. S. Mishima for their support in conducting experiments. The authors are grateful to Mr. N. Kajitani, Ms. A. Sato, Mr. S. Matsuura, and Ms. R. Yoshihara for their cooperation with animal care. The authors would like to thank Editage (www.editage.com) for English language editing.

Received: June 30, 2023; accepted: October 16, 2024; published online: October 25, 2024

## REFERENCES

1. Ringelhan M, Pfister D, O'Connor T, Pikarsky E, Heikenwalder M, The immunology of hepatocellular carcinoma. Nat Immunol 2018; 19:222-32.
2. Zhu W, Zhang X, Yu M, Lin B, Yu C, Radiation-induced liver injury and hepatocyte senescence. Cell Death Discov 2021; 7:244.
3. Weiskirchen R, Tacke F, Cellular and molecular functions of hepatic stellate cells in inflammatory responses and liver immunology. Hepatobiliary Surg Nutr 2014; 3:344-63.
4. Friedman SL, Hepatic stellate cells: protean, multifunctional, and enigmatic cells of the liver. Physiol Rev 2008; 88:125-72.
5. Bataller R, Brenner DA, Liver fibrosis. J Clin Invest 2005; 115: 209-18.
6. Fujita T, Narumiya S, Roles of hepatic stellate cells in liver inflammation: a new perspective. Inflamm Regen 2016:36, 1.
7. Fujita T, Soontrapa K, Ito Y, Iwaisako K, Moniaga CS, Asagiri M, et al., Hepatic stellate cells relay inflammation signaling from sinusoids to parenchyma in mouse models of immune-mediated hepatitis. Hepatology 2016; 63:1325-39.
8. Loo TM, Kamachi F, Watanabe Y, Yoshimoto S, Kanda H, Arai Y, et al., Gut Microbiota Promotes Obesity-Associated Liver Cancer through PGE2-Mediated Suppression of Antitumor Immunity. Cancer Discov 2017; 7:522-38.
9. Yoshimoto S, Loo TM, Atarashi K, Kanda H, Sato S, Oyadomari S, et al., Obesity-induced gut microbial metabolite promotes liver cancer through senescence secretome. Nature 2013; 499:97-101.
10. Barry AE, Baldeosingh R, Lamm R, Patel K, Zhang K, Dominguez DA, et al., Hepatic Stellate Cells and Hepatocarcinogenesis. Front Cell Dev Biol 2020; 8:709.
11. Sasaki S, Influence of the age of mice at exposure to radiation on life-shortening and carcinogenesis. J Radiat Res 1991; 32 Suppl 2:73-85.
12. Shang Y, Kakinuma S, Yamauchi K, Morioka T, Kokubo T, Tani S, et al., Cancer prevention by adult-onset calorie restriction after infant exposure to ionizing radiation in B6C3F1 male mice. Int J Cancer 2014; 135:1038-47.
13. Mederacke I, Dapito DH, Affo S, Uchinami H, Schwabe RF, High-yield and high-purity isolation of hepatic stellate cells from normal and fibrotic mouse livers. Nat Protoc 2015; 10:305-15.
14. Weiskirchen S, Tag CG, Sauer-Lehnen S, Tacke F, Weiskirchen R, Isolation and Culture of Primary Murine Hepatic Stellate Cells. Methods Mol Biol 2017; 1627:165-91.
15. Tan KS, Kulkeaw K, Nakanishi Y, Sugiyama D, Expression of cytokine and extracellular matrix mRNAs in fetal hepatic stellate cells. Genes Cells 2017; 22:836-44.
16. Uyama N, Zhao L, Van Rossen E, Hirako Y, Reynaert H, Adams DH, et al., Hepatic stellate cells express synemin, a protein bridging intermediate filaments to focal adhesions. Gut 2006; 55:1276-89.
17. Livak KJ, Schmittgen TD, Analysis of relative gene expression data using real-time quantitative PCR and the 2(-Delta Delta C (T)) Method. Methods 2001; 25:402-8.

18. Geerts A, History, heterogeneity, developmental biology, and functions of quiescent hepatic stellate cells. Semin Liver Dis 2001; 21:311-35.
19. Shang L, Hosseini M, Liu X, Kisseleva T, Brenner DA, Human hepatic stellate cell isolation and characterization. J Gastroenterol 2018; 53:6-17.
20. Kim BM, Abdelfattah AM, Vasan R, Fuchs BC, Choi MY, Hepatic stellate cells secrete Ccl5 to induce hepatocyte steatosis. Sci Rep 2018; 8:7499.
21. Myojin Y, Hikita H, Sugiyama M, Sasaki Y, Fukumoto K, Sakane S, et al., Hepatic Stellate Cells in Hepatocellular Carcinoma Promote Tumor Growth Via Growth Differentiation Factor 15 Production. Gastroenterology 2021; 160:1741-54 e16.
22. Chen Y, Zhou P, Deng Y, Cai X, Sun M, Sun Y, et al., ALKBH5-mediated m(6) A demethylation of TIRAP mRNA promotes radiation-induced liver fibrosis and decreases radiosensitivity of hepatocellular carcinoma. Clin Transl Med 2023; 13:e1198.
23. Sasaki S, Fukuda N, Temporal variation of excess mortality rate from solid tumors in mice irradiated at various ages with gamma rays. J Radiat Res 2005; 46:1-19.
24. Ozasa K, Shimizu Y, Suyama A, Kasagi F, Soda M, Grant EJ, et al., Studies of the mortality of atomic bomb survivors, Report 14, 1950-2003: an overview of cancer and noncancer diseases. Radiat Res 2012; 177:229-43.
25. Braunersreuther V, Viviani GL, Mach F, Montecucco F, Role of cytokines and chemokines in non-alcoholic fatty liver disease. World J Gastroenterol 2012; 18:727-35.
26. Schwabe RF, Bataller R, Brenner DA, Human hepatic stellate cells express CCR5 and RANTES to induce proliferation and migration. Am J Physiol Gastrointest Liver Physiol 2003; 285:G949-58.
27. Zeng Z, Lan T, Wei Y, Wei X, CCL5/CCR5 axis in human diseases and related treatments. Genes Dis 2022; 9:12-27.
28. Sugihara T, Murano H, Nakamura M, Ichinohe K, Tanaka K, Activation of interferon-stimulated genes by gamma-ray irradiation independently of the ataxia telangiectasia mutated-p53 pathway. Mol Cancer Res 2011; 9:476-84.
29. Wang L, Jiang J, Chen Y, Jia Q, Chu Q, The roles of CC chemokines in response to radiation. Radiat Oncol 2022; 17:63.
30. Mackenzie KJ, Carroll P, Martin CA, Murina O, Fluteau A, Simpson DJ, et al., cGAS surveillance of micronuclei links genome instability to innate immunity. Nature 2017; 548:461-65.
31. Purbey PK, Scumpia PO, Kim PJ, Tong AJ, Iwamoto KS, McBride WH, et al., Defined Sensing Mechanisms and Signaling Pathways Contribute to the Global Inflammatory Gene Expression Output Elicited by Ionizing Radiation. Immunity 2017; 47:421-34 e3.
32. Zheng Z, Jia S, Shao C, Shi Y, Irradiation induces cancer lung metastasis through activation of the cGAS-STING-CCL5 pathway in mesenchymal stromal cells. Cell Death Dis 2020; 11:326.
33. Singh SK, Mishra MK, Rivers BM, Gordetsky JB, Bae S, Singh R, Biological and Clinical Significance of the CCR5/CCL5 Axis in Hepatocellular Carcinoma. Cancers (Basel) 2020; 12.
34. Kawahara A, Kanno K, Yonezawa S, Otani Y, Kobayashi T, Tazuma S, et al., Depletion of hepatic stellate cells inhibits hepatic steatosis in mice. J Gastroenterol Hepatol 2022; 37:1946-54.
35. Ochoa-Callejero L, Perez-Martinez L, Rubio-Mediavilla S, Oteo JA, Martinez A, Blanco JR, Maraviroc, a CCR5 antagonist, prevents development of hepatocellular carcinoma in a mouse model. PLoS One 2013; 8:e53992.
36. Cheng Y, Yamagishi R, Nonaka Y, Sato-Matsubara M, Kawada N, Ohtani N, Non-heat-stressed Method to Isolate Hepatic Stellate Cells From Highly Steatotic Tumor-bearing Liver Using CD49a. Cell Mol Gastroenterol Hepatol 2022; 14:964-66 e9.